Article:
Bai, L, Yang, Z, Shen, X et al. (3 more authors) (2022) Startup characteristics of an ammonia loop heat pipe with a rectangular evaporator. Heat and Mass Transfer, 58 (5). pp. 813-831. ISSN 0947-7411

https://doi.org/10.1007/s00231-021-03139-1

Startup characteristics of an ammonia loop heat pipe with a rectangular evaporator

Lizhan Bai[a], Zehui Yang[a], Xiaobin Shen[a,*], Yuandong Guo[a],

Guiping Lin[a], Dongsheng Wen[a, b]

[a]Laboratory of Fundamental Science on Ergonomics and Environmental Control, School of Aeronautic Science and Engineering, Beihang University, Beijing 100191, PR China

[b]School of Chemical and Process Engineering, University of Leeds, Leeds, LS2 9JT, UK

Abstract: Flat-plate loop heat pipe (FLHP) is a passive two-phase heat transfer device. Comparing with traditional LHP with a cylindrical evaporator, it can be directly connected to a flat heat source without the employment of a saddle, which can effectively reduce the system thermal resistance and enhance the temperature uniformity. In this work, a stainless steel-ammonia FLHP was developed, and extensive experiments have been conducted to investigate its startup characteristics with the evaporator in the horizontal and vertical positions. Experimental results show that the FLHP exhibits excellent startup performance. It can successfully start up at a small heat load as low as 2 W with no obvious temperature overshoot. In a wide power range of 5-35 W, the FLHP generally starts up in only one situation, much simpler than the startup of a LHP with a cylindrical evaporator. For this rectangular evaporator, the heat leak from the evaporator to the compensation chamber (CC) becomes very small. As a result, the vapor can easily exit the condenser in most cases in the power range of 5-35 W, leading to a 100 % utilization efficiency of the condenser and the resultant satisfactory thermal performance of the FLHP. In addition, the startup performance and the system thermal resistance of the FLHP are insensitive to the evaporator orientation, promising great application potential in future electronics cooling.

Keywords: loop heat pipe; evaporator; startup; heat transfer; orientation

* Corresponding author. Tel.: +86 10 8233 8600; Fax: +86 10 8233 8600

E-mail address: shenxiaobin@buaa.edu.cn

1 Introduction

As an advanced two-phase heat transfer device, loop heat pipe (LHP) makes use of the evaporation and condensation cycle of a working fluid to realize efficient heat transfer over a long distance [1-3]. It typically consists of an evaporator, a vapor line, a condenser, a liquid line and a compensation chamber (CC) [4-6]. The porous wick located in the evaporator provides sufficient capillary force to drive the working fluid circulation in the loop where no external power is needed [7-9]. The working principle of a LHP is quite similar to that of a conventional heat pipe. However, through significant structural improvement such as local installment of the porous wick and separation of the liquid/vapor flow, LHP holds many advantages over conventional heat pipe mainly including longer heat transfer distance, larger heat transfer capacity, stronger anti-gravity capability and more flexible thermal link [10-12]. As a result, LHP has a wide range of applications especially in the aerospace field where great success has been achieved in a variety of space missions in the past several decades [13-16].

With the rapid development of communication and telecommunication industry, heat dissipation of electronic equipment has increasingly become an urgent issue to be addressed [17, 18]. It is a feasible solution to apply LHPs to realize the heat dissipation of high power density electronic equipment. At present, studies on the LHP with a cylindrical evaporator are relatively adequate. However, the thermal contact surface of electronic equipment is generally flat, and in practical applications, a saddle is necessarily employed outside the cylindrical evaporator of the LHP to ensure its interaction with the electronic devices [19, 20]. The saddle is usually made of metal materials with high thermal conductivity [21, 22]. The thermal resistance of the system would increase due to the existence of the thermal contact resistance between the evaporator casing and the saddle. Another obvious disadvantage of the cylindrical evaporator is that the thermal flow path between the evaporation interface at the outer surface of the wick and the heater surface is not uniform, which leads to uneven temperature distribution of the heat source [23].

Flat-plate loop heat pipe (FLHP) was developed since its evaporator surface can be directly connected to the electronic equipment without the employment of an additional saddle [24, 25]. According to the relative position between the evaporator and the CC, FLHP can be generally divided into two categories: the upper-lower type and the left-right type [26, 27]. The advantage of the upper-lower type is its sufficient liquid supply from the CC to the evaporator; while the disadvantage is that the heat leak from the evaporator to the CC is quite large, making the FLHP difficult to start up especially at small heat loads. In addition, the evaporator with the upper-lower type usually has a large thickness, which is not suitable for applications in a restricted space. For the left-right type, an evaporator with desirable thickness can be achieved, and at the same time, the heat leak from the evaporator to the CC is relatively small, which is beneficial to the startup performance. However, the pressure drop of liquid flow in the evaporator with the left-right type becomes obviously large, which results in significant reduction of the heat transfer capacity of the FLHP.

To date, FLHP has been studied by quite a few researchers, both theoretically and experimentally, as briefly reviewed below. Anand et al. [28] developed a miniature LHP with an upper-lower type disk-shaped evaporator, and correlated the results of the visualization studies of the working fluid in the CC. The evaporator was made of aluminum alloy, the capillary wick was made of nickel powder, and the CC was made of stainless steel. Acetone, methanol, n-pentane and ethanol were used as the working fluid separately, and the results showed that n-pentane had the lowest operating temperature whereas methanol had the broadest heat load range. Zhang et al. [29] investigated the operating characteristics of a stainless steel-ammonia LHP with an upper-lower type disk-shaped evaporator. A biporous wick made of sintered nickel powders was used to produce the capillary force. The heat transfer distance was 1.6 m and the allowable heater surface temperature was below 70 °C. It turned out to operate under a heat load ranging from 2.5 W to 180 W (heat flux 0.15-10.8 W/cm²) at the heat sink temperature of -10 °C. Noriyuki et al. [30] developed a LHP with an upper-lower type rectangular evaporator which was made of

stainless steel. A polytetrafluoroethylene wick and a stainless steel wick were analyzed in the experimental tests with pure water as the working fluid. The FLHP could operate successfully under the 0.52 m anti-gravity condition at a constant heat sink temperature of 80 °C. As the heat source temperature was limited below 180 °C, the FLHP with the polytetrafluoroethylene wick could transfer a heat load of 650 W with the thermal resistance of 0.071 K/W, while the FLHP with the stainless steel wick could transfer a heat load of 700 W and the thermal resistance was 0.073 K/W. Zhang et al. [31] fabricated a stainless steel-ammonia FLHP with the evaporator of the left-right type. Test results indicated that there were only two startup situations for the FLHP. A superheat degree of above 10 °C was required to initiate the nucleate boiling in the evaporator when the vapor grooves were flooded by liquid. However, it could start up immediately when there existed vapor in the vapor grooves.

According to the analysis above, most studies on the FLHPs reported in the open literatures focus on the evaporator of the upper-lower type, and sufficient investigation on the thermal performance and characteristics has been carried out. For the FLHPs with the evaporator of the left-right type, it is more suitable for the applications in a restricted space [32]. In addition, it generally shows excellent startup performance even at very small heat loads due to significantly reduced heat leak from the evaporator to the CC. However, the relevant studies on the thermal performance of the FLHPs with the evaporator of the left-right type are obviously inadequate, and there is still a lack of extensive understanding on the operation mechanism and performance of this type of LHP. In particular, a systematic study on the startup performance and characteristics is of great importance, since successful startup is the prerequisite to realize a stable and reliable operation of the LHP. In order to push forward its practical applications, it is quite necessary to first reveal its startup characteristics and identify the relevant influencing factors, which forms the main objective of the this work.

2 Experimental system

Fig. 1 shows the experimental setup in this work. The FLHP investigated here was composed of a rectangular

evaporator, vapor/liquid lines, a condenser, and a CC. The detailed structure of the evaporator and CC is presented in Fig. 2. The reinforced structure can ensure that obvious deformation will not occur during operation. The evaporator wick was made of nickel powders, and no secondary wick was used in the test. In the experiment, the heat source was simulated by a ceramic electric resistance heater measuring 5.0×5.0 cm (L×W), which was directly attached to the evaporator surface. The contact surface was evenly coated with a layer of thermal conductive silicone grease to reduce the contact thermal resistance. The ceramic heater was connected to a DC power supply, and the output power can be continuously adjusted in the range of 0-1000 W with an uncertainty of 5.0 %.

In this work, all the components of the FLHP were made of stainless steel except that the porous wick was made of nickel powders. Ammonia was chosen as the working fluid due to its excellent thermophysical properties in the operating temperature range from 0 to 60 ℃ [31, 33]. Table 1 lists the geometric parameters of the FLHP where OD and ID represent the outer and inner diameters, respectively. As shown in Fig. 3, the condenser line was embedded into the bottom surface of a finned radiator measuring 35.0×20.0×3.7 cm (L×W×H), where the heat was dissipated directly to the ambient in the form of air natural convection. Table 2 provides the basic parameters of the finned radiator made of aluminum alloy. All the components were not insulated in order to get maximum cooling efficiency.

Fig. 3 shows the system diagram of the FLHP and the locations of the thermocouples in the experiment. Eleven type-T thermocouples with a maximum measurement error of ± 0.5 ℃ were employed to monitor the temperature profiles along the loop. Note that TC3 was located on the bottom surface of the evaporator, opposite to TC1, and TC11 was on the bottom surface of the CC, opposite to TC10. Temperature data collected by the thermocouple was recorded, displayed, and stored in a PC through a data acquisition system (Agilent 34970A) at each five seconds. The measurement points of the thermocouples were covered by a layer of thermal insulation material to

reduce the heat exchange with the ambient. Since the wall thickness of each FLHP part was no more than 1.0 mm, the measured wall temperature should be very close to the temperature of the working fluid inside.

3 Experimental results and discussions

Startup performance is a very important aspect in evaluating the LHP working performance, and successful startup is the first issue to be resolved in the LHP practical applications. The startup of LHP is a complex dynamic process beginning from the application of a heat load to the evaporator until the attainment of the steady state of every component, accompanied by a variety of phenomena such as evaporation, boiling, condensation and liquid/vapor redistribution in the loop [34, 35].

Generally LHP can realize self-start without employing any auxiliary measures. However, when the startup heat load is relatively small, the self-start process may last for a long time, accompanied by a sharp rise in the evaporator temperature. In fact, the startup of a LHP can be affected by a wide variety of factors, especially the liquid/vapor distribution in the evaporator and the startup heat load. According to the liquid/vapor distribution in the evaporator in the initial state, four possible startup scenarios have been identified, as listed in Table 3. It has been reported that, in situation 1, the liquid in the vapor grooves must be superheated before the phase change can occur there when a heat load is applied to the evaporator. In situation 2, LHP starts up the most easily since liquid will start evaporating once the heat load is applied to the evaporator. In situation 3, the heat leak from the evaporator to the CC is the largest, so the LHP is generally difficult to start up. The startup in situation 4 is similar to that in situation 2, except that the heat leak from the evaporator to the CC becomes larger [7, 36]. According to Ref. 22, since FLHP has no evaporator core inside the evaporator, there will be only two startup scenarios, i.e., the situations 1 and 2. When vapor exists in the vapor grooves, FLHP will start up immediately; whereas an obvious superheat is required to initiate the nucleate boiling for a startup when the vapor grooves are filled by liquid. In this work, much different experimental results have been observed, as

reported and analyzed below.

3.1 Horizontal startup

1) Startup at 2 W

Fig. 4 shows the temperature change of some key points along the loop when an input power of 2 W was applied to the evaporator. The ambient air was used as the heat sink with a nearly constant temperature of 20.5 ℃, and air natural convection was used for heat dissipation. Each part of the system, including the evaporator, CC and condenser, was placed in a horizontal plane, i.e., no adverse elevation or gravity assistance existed.

According to Fig. 4, at the initial state, all the components of the FLHP remained nearly at the ambient temperature. When an input power of 2 W was applied to the electric heater, its temperature (TC1) together with the temperature at the upper surface of the evaporator (TC2) rose rapidly. At the same time, the temperature at the evaporator outlet (TC4) also rose quickly following the evaporator temperature (TC2). It indicated that vapor should exist in the vapor grooves, and evaporation occurred once the heat load was applied to the evaporator. Then the generated vapor flowed out of the evaporator, causing an immediate increase of the temperature at the evaporator outlet (TC4).

It should be noted that the temperature at the upper surface of the CC (TC10) also rose quickly, closely following the evaporator temperature (TC2). It reflects that the energy input into the CC seems relatively large. In the authors' opinion, the energy input into the CC mainly includes two parts: one part is the heat leak from the evaporator through the thermal conduction of both the evaporator casing and the wick; and the other is the compression work to the vapor space of the CC due to the pressure transfer from the evaporator. The former always exists during the startup process, but the latter only exists during obvious liquid/vapor redistribution process in the loop. For instance, when there is no working fluid flow in the loop or the loop nearly reaches the

steady state, the compression work to the vapor space of the CC will be rather small and can be generally neglected.

The temperature at the condenser inlet (TC5) rose quickly, closely following the evaporator temperature (TC2), indicating the generated vapor entered the condenser. After a while, the temperature rise of TC4 became very slow, and it gradually reached a steady state. The temperature of TC6 always remained constant at the ambient temperature, indicating the vapor did not reach the point of TC6. It can be inferred that the two-phase zone in the condenser is very small, resulting in a much reduced utilization efficiency of the condenser. Based on the energy balance analysis, it is well recognized that the small utilization efficiency of the condenser is closely associated with the large heat leak from the evaporator to the CC.

In fact, the heat leak from the evaporator to the CC is strongly dependent on the liquid/vapor distribution in the evaporator/CC. The liquid/vapor distribution in the evaporator/CC is presented in Fig. 5 (a). Due to the thin thickness of the evaporator, the length from the end of the vapor grooves to the CC, i.e., the barrier layer or transition zone, should not be designed too long. Otherwise, the liquid has to flow through a long distance in a small cross-section, which will cause obviously increased flow resistance in the capillary wick, adversely affecting the thermal performance and heat transfer capacity of the FLHP. If the liquid in the CC does not submerge the capillary wick during the startup, the heat leak from the evaporator to the CC will be relatively large. That is because the heat flow is first transferred through the thermal conduction of the barrier layer of the wick, then it is absorbed by liquid evaporation at the side surface of the wick, and the generated vapor flows into the vapor region in the CC, causing an immediate temperature rise of the CC. The more side surface of the wick exposes to the vapor region, the more heat leak exists from the evaporator to the CC.

Fig. 6 shows the temperature profile for another startup when the input power was 2 W. The operating conditions were all the same as those in Fig. 4. As shown in Fig. 6, the initial temperatures of the FLHP

components were nearly the same as the ambient temperature. With an input power of 2 W applied to the electric heater, the heater temperature (TC1) together with the temperature at the upper surface of the evaporator (TC2) began to rise quickly. However, the temperatures at the evaporator outlet (TC4) and the upper surface of the CC (TC10) remained unchanged, which indicated that the vapor grooves were filled with liquid, and a certain superheat was required to initiate the nucleate boiling there. At the same time, the liquid in the CC submerged the capillary wick, and the heat leak from the evaporator to the CC was very small.

When the heater temperature reached about 22 °C, nucleate boiling was initiated, accompanied by a sudden drop of the evaporator temperature (TC2) and simultaneous increase of the temperatures at the evaporator outlet (TC4) and the upper surface of the CC (TC10). It should be noted that the sudden increase of TC10 should be due to the compression work from the evaporator rather than the heat leak from the evaporator. After a short period, the temperature at the condenser inlet (TC5) rose sharply, closely following the evaporator temperature, which indicated that the vapor had entered the condenser. With the circulation of the working fluid in the loop, the temperatures of TC6, TC7 and TC8 at the condenser experienced a sudden increase in sequence, reflecting that the vapor front reached deep in the condenser, and the liquid/vapor two-phase zone occupied a large portion of the condenser, quite different from the case in Fig. 4. In the authors' understanding, the large utilization efficiency of the condenser in Fig. 6 is due to the small heat leak from the evaporator to the CC. In Fig. 6, the liquid in the CC fully submerged the capillary wick, as shown in Fig. 5(b), and under this condition, liquid evaporation at the side surface of the wick can no longer occur, replaced by liquid single phase convection. As a result, the heat leak from the evaporator to the CC became very weak, which is beneficial to the performance enhancement of the FLHP. Eventually, the evaporator and the CC reached obviously lower steady state operating temperatures of about 21 °C.

2) Startup at 5 W

Fig. 7 shows the temperature change of some key points along the loop when an input power of 5 W was applied, where the other operating conditions were all the same as those in Fig. 4. At the initial state, all the components of the FLHP were at the ambient temperature. With an input power of 5 W applied to the electric heater, the heater temperature (TC1) together with the temperatures at the upper surface of the evaporator (TC2), the evaporator outlet (TC4), and the condenser inlet (TC5) rose quickly. This showed that vapor was generated instantaneously in the vapor grooves and flowed into the condenser through the vapor line. The temperature of TC1 dropped abruptly due to a large amount of heat taken away by the phase change process of working fluid in the evaporator, and then the temperature continued to increase at a low rate. It can be inferred that vapor should exist in the vapor grooves, and liquid evaporation occurred once a heat load was applied to the evaporator. At the same time, similar to the phenomenon in Fig. 4, the temperature at the upper surface of the CC (TC10) also increased quickly.

With the circulation of the working fluid in the loop, the temperatures of TC6, TC7 and TC8 at the condenser and TC9 at the CC inlet experienced a sudden increase in sequence, reflecting that the vapor exited the condenser and reached the CC inlet, and under this condition, the condenser was fully utilized with a utilization efficiency of 100%. Eventually, the evaporator reached a steady state operating temperature of about 23 ℃.

3) Startup at 10 W and 20 W

Figs. 8 and 9 show the temperature change of some key points along the loop with an input power of 10 W and 20 W respectively, where the other operating conditions were all the same as those in Fig. 4. In Fig. 8, once the input power was applied to the electric heater, the heater temperature (TC1) and the temperatures at the evaporator outlet (TC4) and the condenser inlet (TC5) rose quickly, indicating that vapor was generated instantaneously in the vapor grooves and flowed into the condenser through the vapor line. These phenomena were quite similar to those in Fig. 7. Due to the larger heat load, the temperature of TC1 did not drop suddenly,

but increased gradually at a lower rate.

Similar to the case in Fig. 7, after a short time, the temperatures of TC6, TC7 and TC8 at the condenser and TC9 at the CC inlet experienced a sudden increase in sequence, reflecting that the vapor exited the condenser and reached the CC inlet, and under this condition, the condenser was fully utilized. Compared with the low power of 5 W, the time to reach the steady state was significantly shortened at 10W. For instance, TC9 rose suddenly at about 70 min at an input power of 5 W; while it was reduced to about 40 min at an input power of 10 W. In the steady state, the difference between the highest and lowest temperatures on the FLHP did not exceed 2 °C, which proved that the FLHP had excellent temperature uniformity on the whole loop.

With an input power of 20 W, the startup process was quite similar to that when the input power was 10 W. The difference was that the startup time was further reduced. For instance, TC9 rose suddenly at about 40 min at an input power of 10 W; while it was further reduced to about 20 min at an input power of 20 W, as shown in Fig. 9.

4) Startup at 35 W

When the input power was increased to 35 W, the temperature change of some key points along the loop are presented in Fig. 10. Once the input power was applied, the heater temperature (TC1), together with the temperatures at the evaporator outlet (TC4), and the condenser inlet (TC5) rose quickly, quite similar to the case in Fig. 8. As shown in Fig. 10, the temperatures of TCs 6, 7, and 8 on the condenser rose rapidly with the circulation of the working fluid, but the temperature at the CC inlet (TC9) was not as high as that in Fig. 8, which was obviously lower than the saturation temperature of the FLHP. The reason might be the increase of the heat leak from the evaporator to the CC at a larger heat load, and correspondingly the working fluid at the CC inlet needs a larger subcooling degree to compensate the heat leak from the evaporator to the CC, in order to achieve the energy balance of the CC.

3.2 Vertical startup

In order to investigate the influence of evaporator orientation on the startup of the FLHP, extensive experiments have been carried out. In the experiment, the evaporator was placed in the vertical position with the CC located above the evaporator, as shown in Fig. 11. Under this condition, the CC can guarantee sufficient liquid supply to the capillary wick. It should also be noted that the evaporator was about 0.15 m higher than the condenser, i.e., an adverse elevation of 0.15 m existed in the experiments.

1) Startup at 5 W

Fig. 12 shows the temperature change of some key points along the loop when an input power of 5 W was applied, where the other operating conditions were all the same as those in Fig. 7 except that the evaporator was in the vertical position.

According to Fig. 12, at the initial state, all the components of the FLHP were at the ambient temperature. Once an input power of 5 W was applied to the electric heater, the heater temperature (TC1) together with the temperatures at the upper surface of the evaporator (TC2), the evaporator outlet (TC4), and the condenser inlet (TC5) rose quickly. It suggested that vapor was generated instantaneously in the vapor grooves and then flowed into the condenser via the vapor line. It can be inferred that vapor should exist in the vapor grooves, and liquid evaporation occurred once the heat load was applied to the evaporator.

At the same time, the temperatures at the upper and bottom surface of the CC (TC10 and TC11) both experienced a sudden increase, which may be caused by the vapor compression work in the CC due to the pressure transfer from the evaporator. When the evaporator was placed in the vertical attitude, the liquid in the CC will fully submerge the capillary wick, as shown in Fig. 13, and under this condition, liquid evaporation at the side surface of the capillary wick can no longer occur. As a result, the heat leak from the evaporator to the CC should be very small. The CC temperature change was quite different from the case in the horizontal

position. When the evaporator was placed in the horizontal position, the temperature of TC11 generally remained constant, because it mainly reflected the liquid temperature in the CC, whose temperature was insensitive to its pressure. Whereas when the evaporator was placed in the vertical position, both the temperatures of TC10 and TC11 reflected the vapor temperature in the CC.

With the circulation of the working fluid in the loop, the temperatures of TC6, TC7 and TC8 at the condenser and TC9 at the CC inlet experienced a sudden increase in sequence, similar to the case in the horizontal position, reflecting that the vapor exited the condenser and reached the CC inlet, and under this condition, the condenser was fully utilized with a utilization efficiency of 100%. From the point of view of energy balance analysis, the heat leak from the evaporator to the CC should be very small when the evaporator was in the vertical position. Eventually, the evaporator reached a steady state.

The FLHP in Ref. 22 required about 10 ℃ superheat to start up at a low power, while the superheat required for the startup of the FLHP in this work was quite small, and can be generally neglected in most occasions. In the authors' opinion, there are mainly two reasons: first, the superheat required to initiate the nucleate boiling is closely associated with the heating surface morphology, which may differ significantly for different surfaces and manufacture processes; secondly, the small amount of non-condensable gas existing in the vapor grooves or the outer surface of the capillary wick may be beneficial to the nucleation and following liquid evaporation during the startup, considerably reducing the superheat. Taking this point into account, the existence of a small amount of non-condensable seems necessary for the performance enhancement of the startup of the LHP.

2) Startup at 10 W and 20 W

Figs. 14 and 15 show the temperature change of some key points along the loop with an input power of 10 W and 20 W respectively, where the other operating conditions were all the same as those in Fig. 13. In Fig. 14, once the input power was applied to the electric heater, the heater temperature (TC1) and the temperatures at

the evaporator outlet (TC4) and the condenser inlet (TC5) rose quickly, indicating that vapor was generated instantaneously in the vapor grooves and flowed into the condenser through the vapor line. Similar to the case in Fig. 13, after a short period, the temperatures of TC6, TC7 and TC8 at the condenser and TC9 at the CC inlet experienced a sudden increase in sequence, reflecting that the vapor exited the condenser and reached the CC inlet, and under this condition, the condenser was fully utilized. Compared with the low power of 5 W, the time to reach the steady state was obviously shortened at 10W. For instance, TC9 rose suddenly at about 50 min at an input power of 5 W; while it was reduced to about 30 min at an input power of 10 W. In the steady state, the difference between the highest and lowest temperatures on the FLHP did not exceed 2 °C. Therefore the FLHP exhibited excellent temperature uniformity on the whole loop.

With an input power of 20 W, the startup process was quite similar to that when the input power was 10 W. The difference was that the startup time was further reduced. For instance, TC9 rose suddenly at about 30 min at an input power of 10 W; while it was further reduced to about 15 min at an input power of 20 W, as shown in Fig. 15.

3) Startup at 35 W

When the input power was increased to 35 W, the temperature change of some key points along the loop during the startup process is shown in Fig. 16. Once the input power was applied to the heater, the heater temperature (TC1) together with the temperatures at the evaporator outlet (TC4) and the condenser inlet (TC5) rose quickly, indicating that vapor was generated instantaneously in the vapor grooves and flowed into the condenser through the vapor line. After about 2 minutes, the temperatures of TC6, TC7, and TC8 began to increase rapidly. The temperature rise of TC9 in the steady-state was also lower than that in Fig. 15, quite similar to the case in the horizontal position.

3.3 System thermal resistance

The thermal resistance of the FLHP system is defined as the thermal resistance from the heat source to the heat sink, which can be expressed by equation (1):

$$R_{sys} = \frac{T_{source} - T_{sink}}{Q_{ap}} \quad (1)$$

where T_{source} is the temperature of the electric heater, T_{sink} is the heat sink temperature, which is equal to the ambient temperature in this work, and Q_{ap} is the input power applied to the electric heater.

The uncertainty of the system thermal resistance R_{sys} can be estimated using equation (2):

$$\frac{\Delta R_{sys}}{R_{sys}} = \sqrt{\left(\frac{\Delta T_{source}}{T_{source} - T_{sink}}\right)^2 + \left(\frac{\Delta T_{sink}}{T_{source} - T_{sink}}\right)^2 + \left(\frac{\Delta Q_{ap}}{Q_{ap}}\right)^2} \quad (2)$$

where ΔT_{source}, ΔT_{sink}, denote the measurement errors for the temperatures of T_{source} and T_{sink}; ΔQ_{ap} is the measurement error of the input power Q_{ap}. The uncertainty of R_{sys} was estimated to be within 6.0 % in the experimental conditions in this work.

Fig. 17 shows the heat load dependency of the FLHP system thermal resistance. When the FLHP was operating in the horizontal position, the thermal resistance of the system was about 1.04 °C/W at the input power of 5 W. As the input power was increased to 30 W, the thermal resistance of the system gradually decreased to 0.65 °C/W. When the input power reached 35 W, due to the increase of the heat leak from the evaporator to the CC, the vapor front receded to some extent, and the thermal resistance of the system increased slightly.

When the FLHP was operating with the evaporator in the vertical position, the thermal resistance of the system exhibited a variation trend quite similar to that in the horizontal position, and the difference in the two curves was very small. It indicated that the FLHP thermal performance was insensitive to the evaporator orientation, and the effect of evaporator orientation on the thermal performance of the FLHP can be generally neglected. That is because with appropriate working fluid inventory in the loop, whether the evaporator is placed in the horizontal or vertical position, the liquid in the CC can always fully submerge the capillary wick

at the steady state in the heat load range of 5-35 W. Under this condition, the difference in the heat leak from the evaporator to the CC when the evaporator is in the horizontal or the vertical orientation is very small. As a result, the final steady state operating temperature of the FLHP will be generally the same, as well as the system thermal resistance.

4 Conclusions

In this work, a stainless steel-ammonia FLHP was designed and fabricated. Extensive experiments have been carried out to investigate its startup performance and characteristics, where the effects of startup heat load and evaporator position were considered. The experimental results well reveal the operation mechanism and performance of the startup, as summarized below:

- The FLHP exhibited excellent startup performance. It can successfully start up in the heat load range of 2-35 W. No startup failure was observed in all the tests, and at the same time no obvious temperature overshoot occurred.
- In the heat load range of 5-35 W, the FLHP only started up in one similar situation: vapor existed in the vapor grooves and liquid in the CC fully submerged the capillary wick, which was much simpler than the startup of a LHP with a traditional cylindrical evaporator.
- Whether the evaporator was in the horizontal or the vertical position, once the heat load was applied, vapor can be generated immediately in the vapor grooves to initiate the working fluid flow in the loop, and no obvious liquid superheat was observed in all the tests.
- For this rectangular evaporator, the heat leak from the evaporator to the CC became very small, and as a result, vapor exited the condenser in most cases, leading to a 100% utilization efficiency of the condenser, which resulted in a very low steady state operating temperature by fully utilizing the cooling capacity of the condenser.

- The startup performance and the system thermal resistance of the FLHP were insensitive to the evaporator orientation, promising great potential in future applications.

Conflict of interest

On behalf of all authors, the corresponding author states that there is no conflict of interest.

Acknowledgements

This work was supported by the National Natural Science Foundation of China (No. 51776012) and the Beijing Natural Science Foundation (No. 3182023).

References

[1] Y. Zhao, N. Wang, T. Yan, J. Liang, H. Chen, Experimental study on operating characteristics of a cryogenic loop heat pipe without additional power consumption, Applied Thermal Engineering. 184 (2021) 116262. https://doi.org/10.1016/j.applthermaleng.2020.116262.

[2] H. Wang, G. Lin, X. Shen, L. Bai, R. Yang, D. Wen, Effect of evaporator/condenser elevations on a loop heat pipe with non-condensable gas, Applied Thermal Engineering. 180 (2020) 115711. https://doi.org/10.1016/j.applthermaleng.2020.115711.

[3] H. Zhang, C. Jiang, Z. Zhang, Z. Liu, X. Luo, W. Liu, A study on thermal performance of a pump-assisted loop heat pipe with ammonia as working fluid, Applied Thermal Engineering. 175 (2020) 115342. https://doi.org/10.1016/j.applthermaleng.2020.115342.

[4] X. Li, B. Xu, G. Zhang, Y. Wang, B. Dai, K. Zhu, S. Liu, Z. Zhang, Experimental investigation on the impact of pressure head of evaporation during the loop heat pipe operation, Applied Thermal Engineering. 185 (2021) 116455. https://doi.org/10.1016/j.applthermaleng.2020.116455.

[5] L. Zhou, Z.G. Qu, G. Chen, J.Y. Huang, J.Y. Miao, One-dimensional numerical study for loop heat pipe with two-phase heat leak model, International Journal of Thermal Sciences. 137 (2019) 467-481. https://doi.org/10.1016/j.ijthermalsci.2018.12.019.

[6] H. Wang, G. Lin, X. Shen, L. Bai, D. Wen, Effect of evaporator tilt on a loop heat pipe with non-condensable gas, International Journal of Heat and Mass Transfer. 128 (2019) 1072-1080. https://doi.org/10.1016/j.ijheatmasstransfer.2018.09.033.

[7] J. Ku, Operating characteristics of loop heat pipes, SAE International. 108 (1999) 503-519. https://doi.org/10.4271/1999-01-2007.

[8] A. Ambirajan, A.A. Adoni, J.S. Vaidya, A.A. Rajendran, D. Kumar, P. Dutta, Loop heat pipes: a review of

fundamentals, operation, and design, Heat Transf. Eng. 33 (2012) 387-405. https://doi.org/10.1080/01457632.2012.614148.

[9] I. Setyawan, N. Putra, I.I. Hakim, Experimental investigation of the operating characteristics of a hybrid loop heat pipe using pump assistance, Applied Thermal Engineering. 130 (2018) 10-16. https://doi.org/10.1016/j.applthermaleng.2017.11.007.

[10] Yu. F. Maydanik, Loop heat pipes, Applied Thermal Engineering. 25 (2005) 635-657. https://doi.org/10.1016/j.applthermaleng.2004.07.010.

[11] K. Nakamura, K. Odagiri, H. Nagano, Study on a loop heat pipe for a long-distance heat transport under anti-gravity condition, Applied Thermal Engineering. 107 (2016) 167-174. https://doi.org/10.1016/j.applthermaleng.2016.06.162.

[12] B. Siedel, V. Sartre, F. Lefèvre, Literature review: Steady-state modelling of loop heat pipes, Applied Thermal Engineering. 75 (2015) 709–723. https://doi.org/10.1016/j.applthermaleng.2014.10.030.

[13] K. Goncharov, O. Golovin, V. Kolesnikov, Z. Xiaoxiang, Development and flight operation of LHP used for cooling nickel-cadmium batteries in Chinese meteorological satellites FY-1, in: Proc. 13th Int. Heat Pipe Conf. Shanghai, China, China Astronautic Publishing House Beijing, 2004.

[14] G. Wang, D. Mishkinis, D. Nikanpour, Capillary heat loop technology: Space applications and recent Canadian activities, Applied Thermal Engineering. 28 (2008) 284-303. https://doi.org/10.1016/j.applthermaleng.2006.02.027.

[15] J. Rodriguez, A. Na-Nakornpanom, In-Flight Performance of the TES Loop Heat Pipe Heat Rejection System - Seven Years In Space, in: 42nd International Conference on Environmental Systems, American Institute of Aeronautics and Astronautics, (2012) 1–10. https://doi.org/10.2514/6.2012-3500.

[16] H. Zhang, G. Li, L. Chen, G. Man, J. Miao, X. Ren, J. He, Y. Huo, Development of Flat-Plate Loop Heat

Pipes for Spacecraft Thermal Control, Microgravity Sci. Technol. 31 (2019) 435-443. https://doi.org/10.1007/s12217-019-09716-8.

[17] M. Bahiraei, S. Heshmatian, Electronics cooling with nanofluids: A critical review, Energy Conversion and Management. 172 (2018) 438–456. https://doi.org/10.1016/j.enconman.2018.07.047.

[18] Li, G. Zhou, T. Tian, X. Li, A new cooling strategy for edge computing servers using compact looped heat pipe, Applied Thermal Engineering. 187 (2021) 116599. https://doi.org/10.1016/j.applthermaleng.2021.116599.

[19] V.G. Pastukhov, Yu.F. Maidanik, C.V. Vershinin, M.A. Korukov, Miniature loop heat pipes for electronics cooling, Applied Thermal Engineering. 23 (2003) 1125-1135. https://doi.org/10.1016/S1359-4311(03)00046-2.

[20] L. Bai, Y. Tao, Y. Guo, G. Lin, Startup characteristics of a dual compensation chamber loop heat pipe with an extended bayonet tube, International Journal of Heat and Mass Transfer. 148 (2020) 119066. https://doi.org/10.1016/j.ijheatmasstransfer.2019.119066.

[21] W. Joung, T. Yu, J. Lee, Experimental study on the loop heat pipe with a planar bifacial wick structure, International Journal of Heat and Mass Transfer. 51 (2008) 1573-1581. https://doi.org/10.1016/j.ijheatmasstransfer.2007.07.048.

[22] L. Bai, J. Fu, G. Lin, C. Zhou, D. Wen, Quiet power-free cooling system enabled by loop heat pipe, Applied Thermal Engineering. 155 (2019) 14-23. https://doi.org/10.1016/j.applthermaleng.2019.03.147.

[23] Z. Zhang, H. Zhang, Z. Ma, Z. Liu, W. Liu, Experimental study of heat transfer capacity for loop heat pipe with flat disk evaporator, Applied Thermal Engineering. 173 (2020) 115183. https://doi.org/10.1016/j.applthermaleng.2020.115183.

[24] Z. Liu, D. Wang, C. Jiang, J. Yang, W. Liu, Experimental study on loop heat pipe with two-wick flat

evaporator, International Journal of Thermal Sciences. 94 (2015) 9-17. https://doi.org/10.1016/j.ijthermalsci.2015.02.007.

[25] D. Wang, Z. Liu, J. Shen, C. Jiang, B. Chen, J. Yang, Z. Tu, W. Liu, Experimental study of the loop heat pipe with a flat disk-shaped evaporator, Experimental Thermal and Fluid Science. 57 (2014) 157-164. https://doi.org/10.1016/j.expthermflusci.2014.04.017.

[26] A.R. Anand, Investigations on effect of noncondensable gas in a loop heat pipe with flat evaporator on deprime, International Journal of Heat and Mass Transfer. 143 (2019) 118531. https://doi.org/10.1016/j.ijheatmasstransfer.2019.118531.

[27] Y. Maydanik, S. Vershinin, M. Chernysheva, S. Yushakova, Investigation of a compact copper–water loop heap pipe with a flat evaporator, Applied Thermal Engineering. 31 (2011) 3533-3541. https://doi.org/10.1016/j.applthermaleng.2011.07.008.

[28] A.R. Anand, A. Jaiswal, A. Ambirajan, P. Dutta, Experimental studies on a miniature loop heat pipe with flat evaporator with various working fluids, Applied Thermal Engineering. 144 (2018) 495-503. https://doi.org/10.1016/j.applthermaleng.2018.08.092.

[29] Z. Zhang, H. Zhang, Z. Ma, Z. Liu, W. Liu, Experimental study of heat transfer capacity for loop heat pipe with flat disk evaporator, Applied Thermal Engineering. 173 (2020) 115183. https://doi.org/10.1016/j.applthermaleng.2020.115183.

[30] N. Watanabe, N. Phan, Y. Saito, S. Hayashi, N. Katayama, H. Nagano, Operating characteristics of an anti-gravity loop heat pipe with a flat evaporator that has the capability of a loop thermosyphon, Energy Conversion and Management. 205 (2020) 112431. https://doi.org/10.1016/j.enconman.2019.112431.

[31] H. Zhang, G. Li, L. Chen, G. Man, J. Miao, X. Ren, J. He, Y. Huo, Development of Flat-Plate Loop Heat Pipes for Spacecraft Thermal Control, Microgravity Sci. Technol. 31 (2019) 435-443.

https://doi.org/10.1007/s12217-019-09716-8.

[32] G.P. Celata, M. Cumo, M. Furrer, Experimental tests of a stainless steel loop heat pipe with flat evaporator, Experimental Thermal and Fluid Science. 34 (2010) 866-878. https://doi.org/10.1016/j.expthermflusci.2010.02.001.

[33] Yu.F. Maydanik, S.V. Vershinin, M.A. Chernysheva, Experimental study of an ammonia loop heat pipe with a flat disk-shaped evaporator using a bimetal wall, Applied Thermal Engineering. 126 (2017) 643-652. https://doi.org/10.1016/j.applthermaleng.2017.07.152.

[34] X. Ji, Y. Wang, J. Xu, Y. Huang, Experimental study of heat transfer and start-up of loop heat pipe with multiscale porous wicks, Applied Thermal Engineering. 117 (2017) 782-798. https://doi.org/10.1016/j.applthermaleng.2017.01.084.

[35] Y. Zhang, T. Luan, H. Jiang, J. Liu, Visualization study on start-up characteristics of a loop heat pipe with a carbon fiber capillary wick, International Journal of Heat and Mass Transfer. 169 (2021) 120940. https://doi.org/10.1016/j.ijheatmasstransfer.2021.120940.

[36] H. Zhang, G. Lin, T. Ding, et al, Investigation of startup behaviors of a loop heat pipe, Journal of Thermophysics and Heat Transfer, 19 (2005) 509-518. https://doi.org/10.2514/1.12008.

Table captions

Table 1 Basic parameters of the tested FLHP

Table 2 Basic parameters of the fin radiator

Table 3 Liquid/vapor distribution in the evaporator

Figure captions

Table 1 Basic parameters of the tested FLHP

Components	Parameters
Length×Width×Height of evaporator/mm	66×51×8
Length×Width×Height of wick/mm	50×49×6
OD/ID×Length of vapor line/mm	3/2×300
OD/ID×Length of condenser/mm	3/2×2700
OD/ID×Length of liquid line/mm	3/2×520
Number×height×width of Grooves/mm	10×1×1
Volume of CC /ml	16.5
Working fluid inventory/g	14.9
Porosity of wick	55 %
Maximum pore radius of wick/μm	1.0

Table 2 Basic parameters of the fin radiator

Items	Parameters
Length × Width × Height of fin radiator /mm	$350 \times 200 \times 42$
Length × Height × Thickness of fins/mm	$350 \times 35 \times 1.5$
Number × Spacing between the fins/mm	34×4.3
Number of fins	35

Table 3 Liquid/vapor distribution in the evaporator

Situations	Vapor grooves/evaporator core
1	Liquid filled/liquid filled
2	Vapor exists/ liquid filled
3	Liquid filled /vapor exists
4	Vapor exists/vapor exists

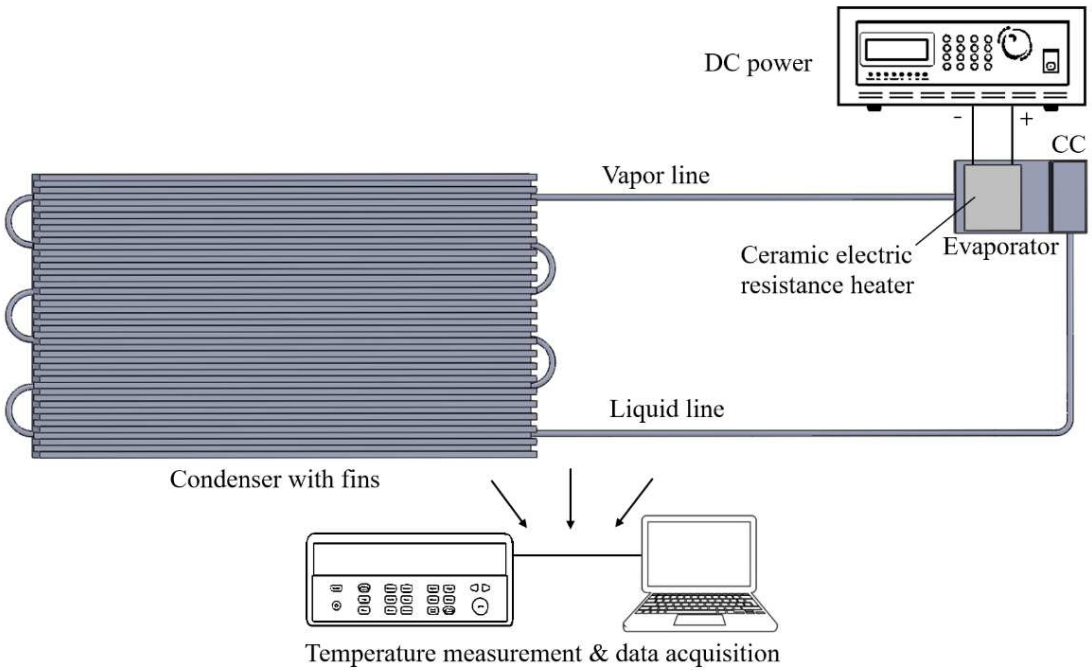

Fig. 1 The experimental system of the FLHP

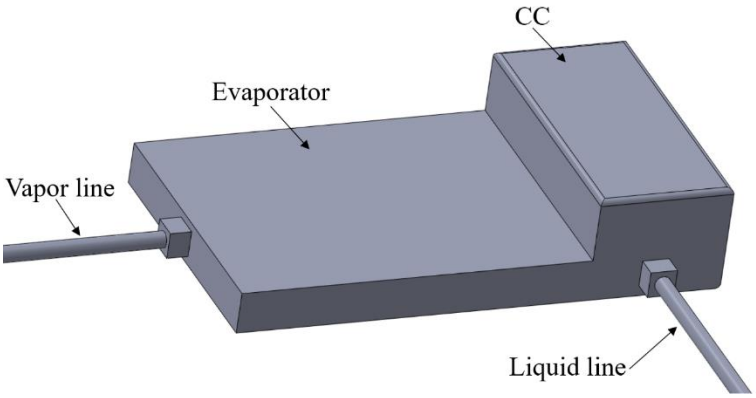

(a) 3D structure of the evaporator/CC

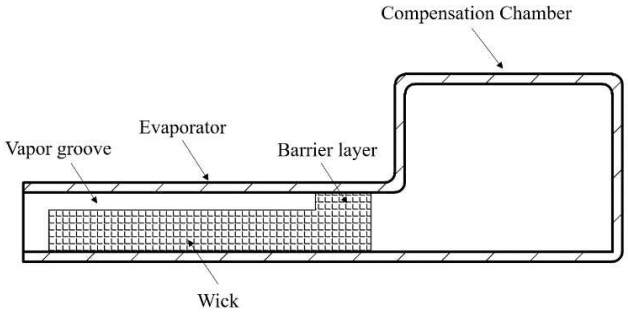

(b) section view A

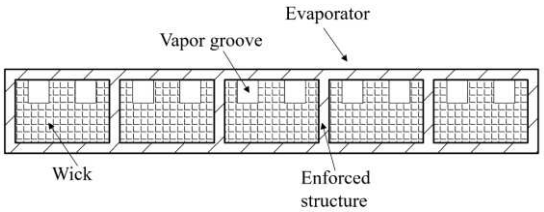

(c) section view B

Fig. 2 Detailed structure of the evaporator/CC of the FLHP

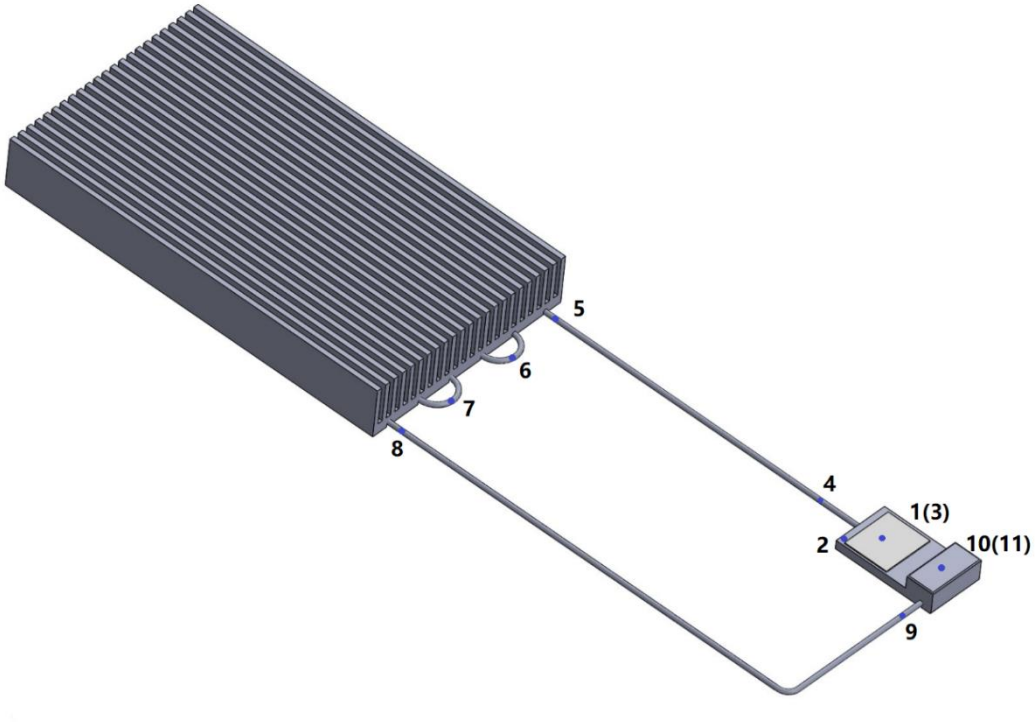

Fig. 3 System diagram of the FLHP and the locations of thermocouple

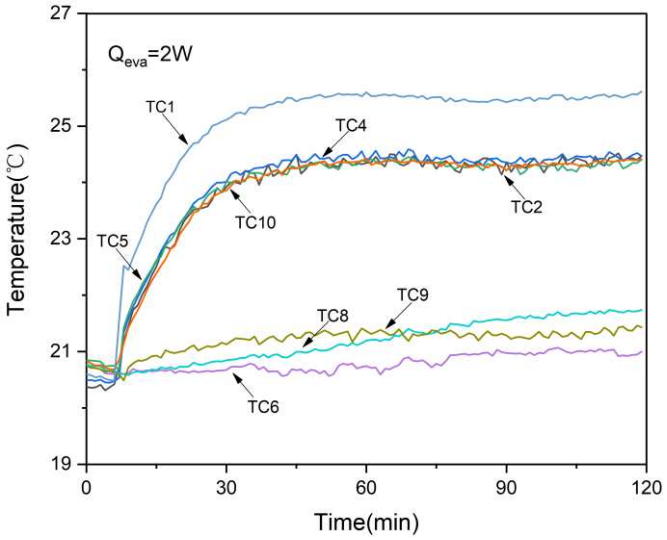

(a) the whole process

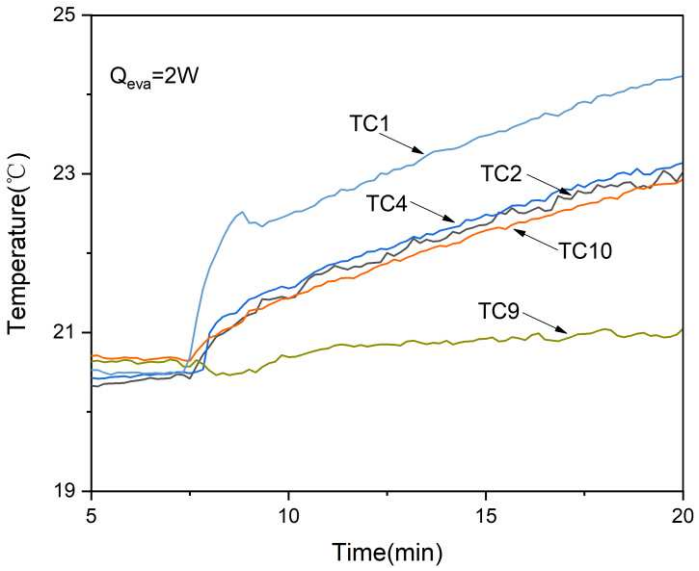

(b) local enlargement

Fig. 4 Horizontal startup with an input power of 2 W in case 1

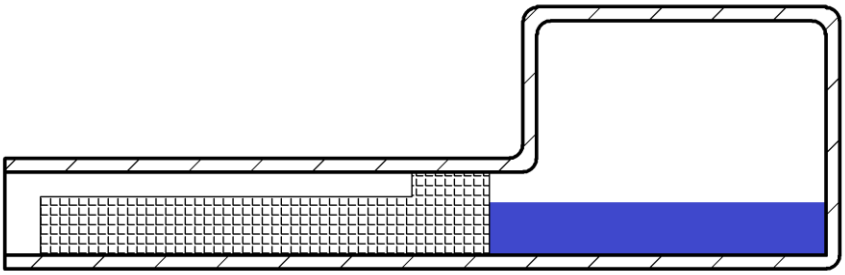

(a) Liquid in the CC does not submerge the wick

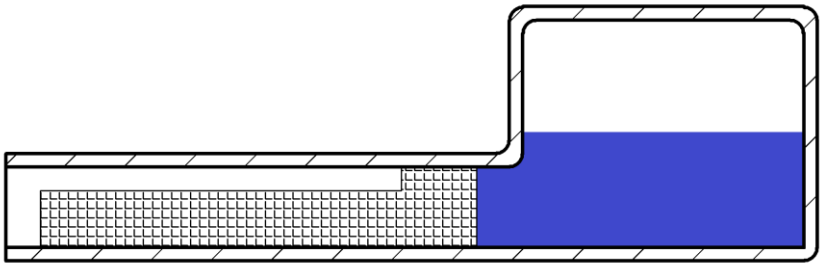

(b) Liquid in the CC fully submerges the wick

Fig. 5 Liquid/vapor distribution in the evaporator/CC of the FLHP

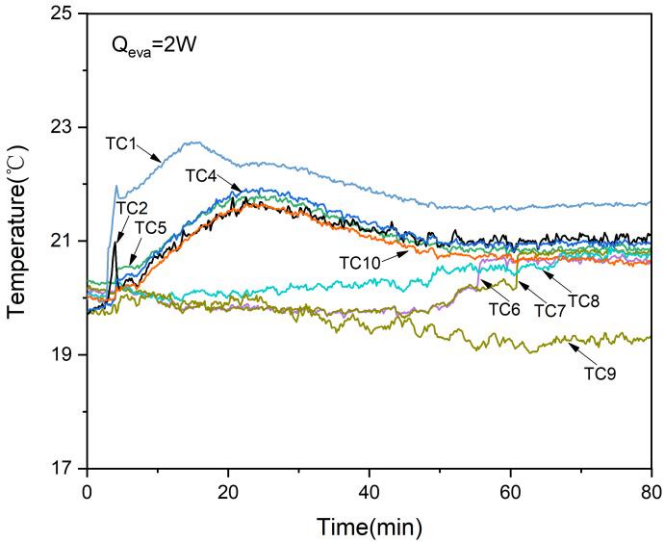

(a) the whole process

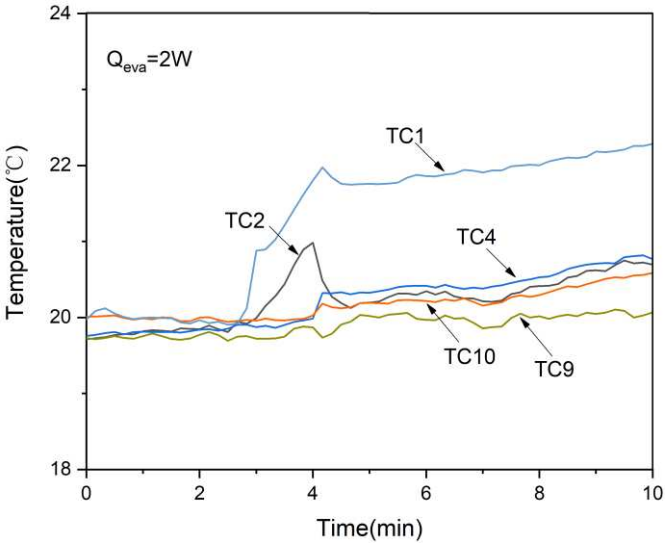

(b) local enlargement

Fig. 6 Horizontal startup with an input power of 2 W in case 2

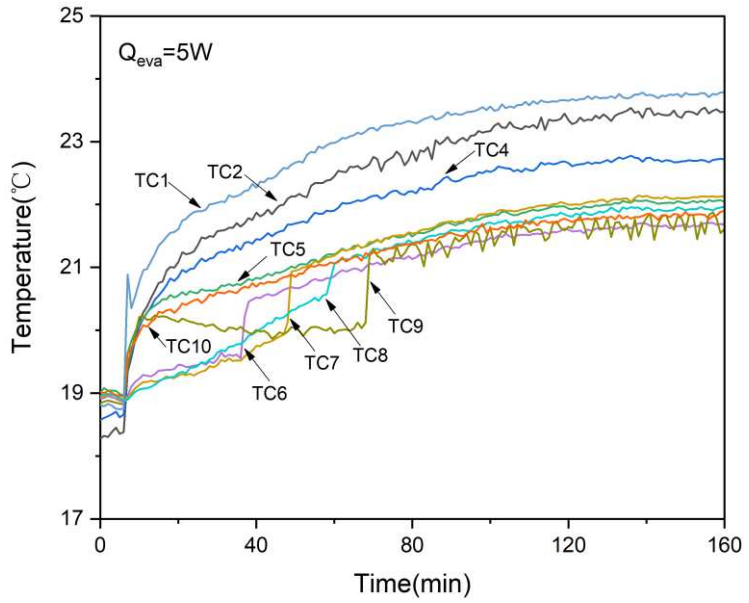

Fig. 7 Startup at horizontal orientation with an input power of 5 W

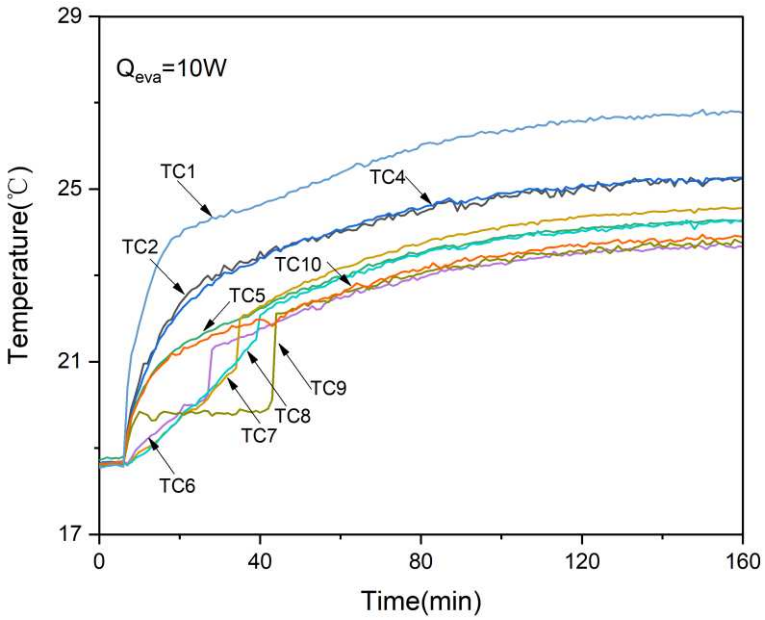

Fig. 8 Startup at horizontal orientation with an input power of 10 W

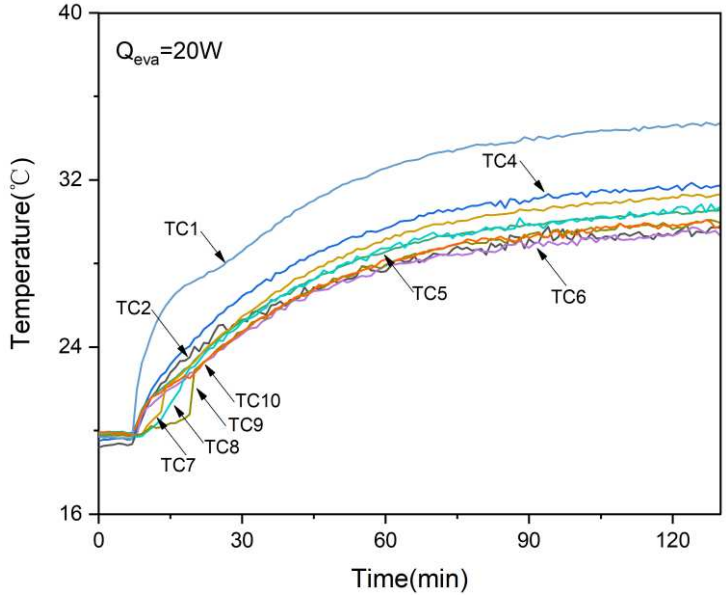

Fig. 9 Startup at horizontal orientation with an input power of 20 W

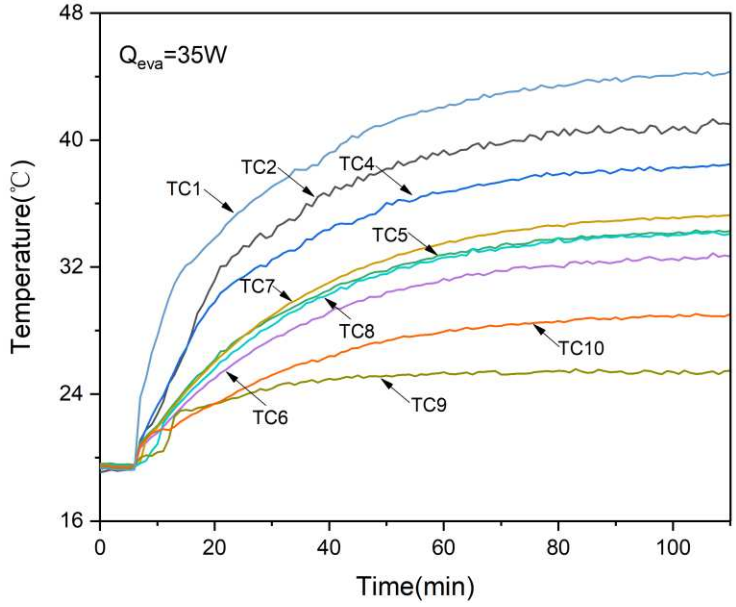

Fig. 10 Startup at horizontal orientation with an input power of 35 W

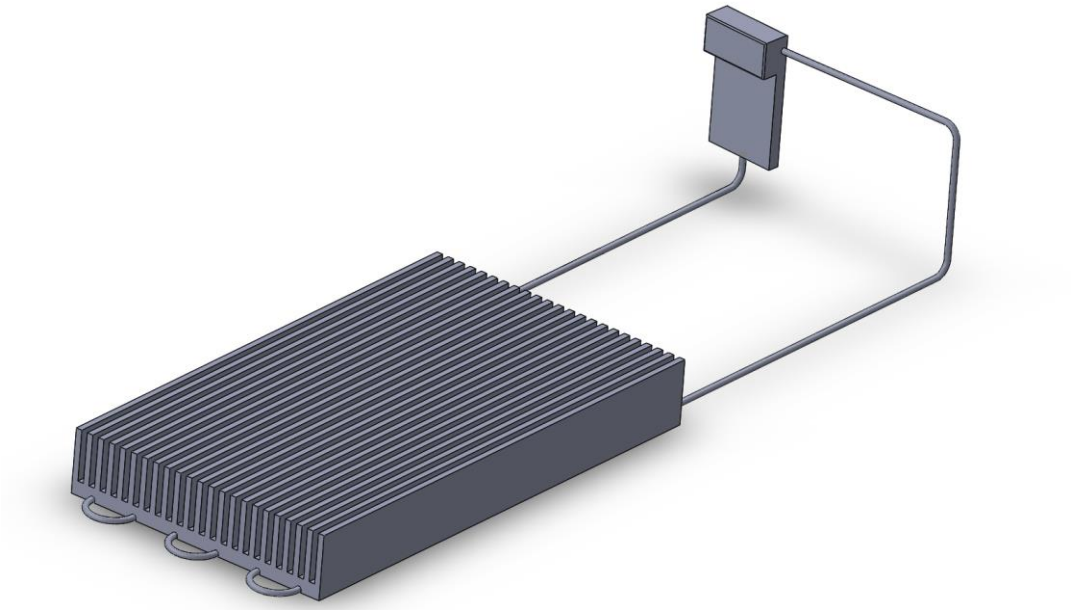

Fig. 11 Schematic of the FLHP with the evaporator in the vertical position

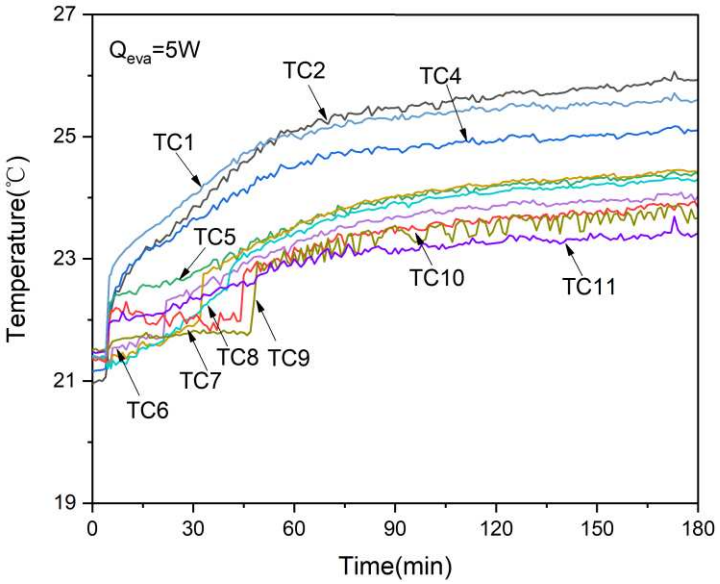

(a) the whole process

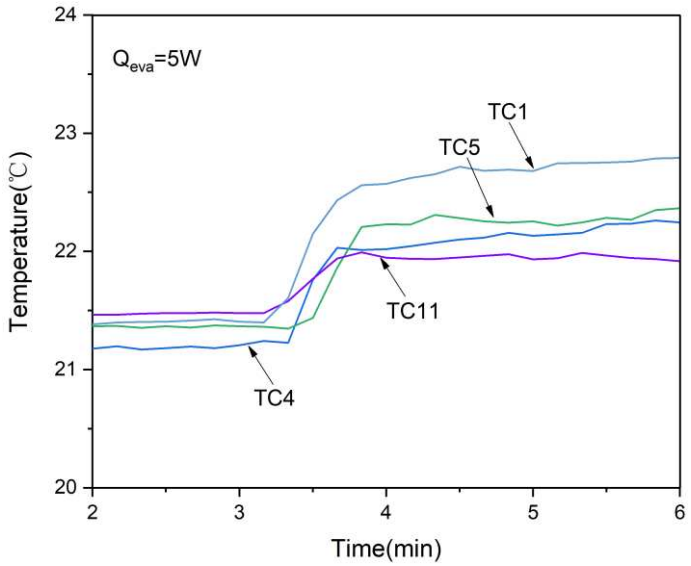

(b) local enlargement

Fig. 12 Startup at vertical orientation with an input power of 5 W

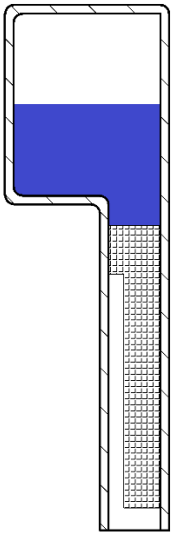

Fig. 13 Liquid/vapor distribution in the evaporator/CC in the vertical orientation

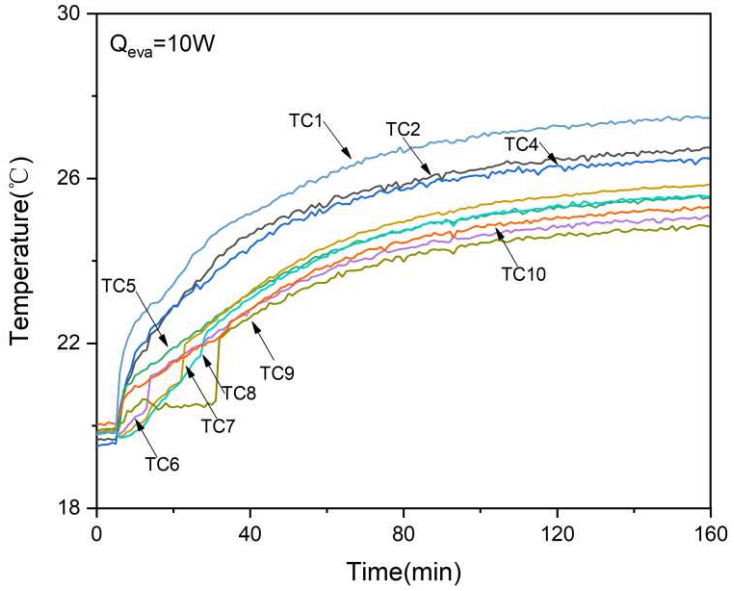

Fig. 14 Startup at vertical orientation with an input power of 10 W

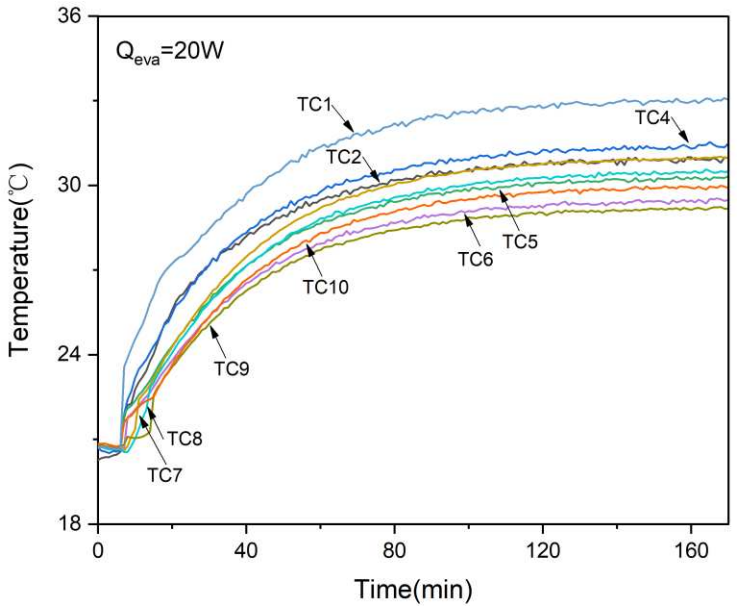

Fig. 15 Startup at vertical orientation with an input power of 20 W

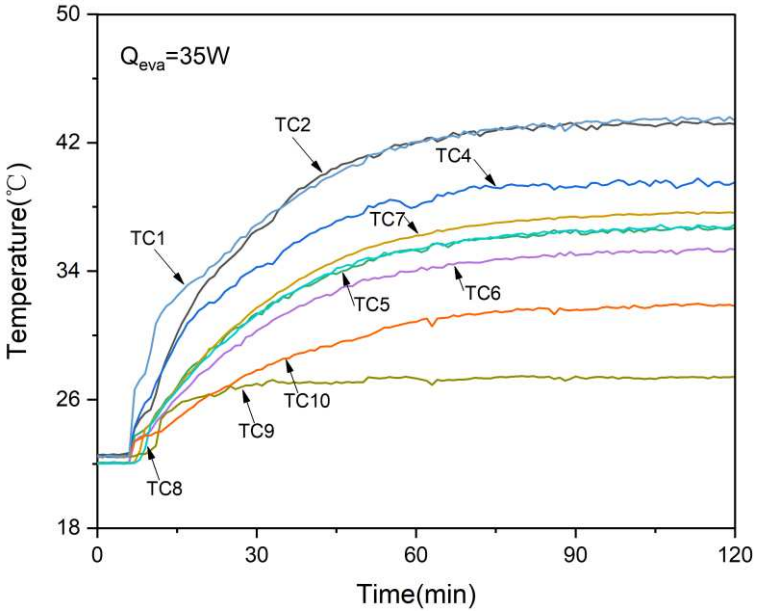

Fig. 16 Startup at vertical orientation with an input power of 35 W

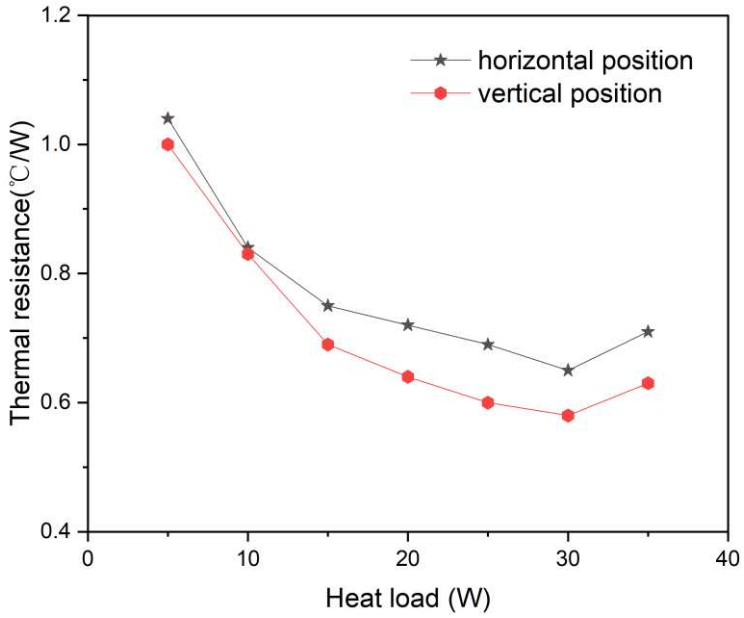

Fig. 17 Heat load dependency of the system thermal resistance